Geophysical Research Letters

RESEARCH LETTER
10.1029/2025GL118481

The Cycles and Dynamical Properties of Convective Outbreaks in Jupiter's Highest Speed Jet From a 55-Year Study

Agustín Sánchez-Lavega[1], José Félix Rojas[1], Jon Legarreta[1], Alberto Mendi-Martos[2], Ricardo Hueso[1], Peio Iñurrigarro[3], Amy A. Simon[4], Michael H. Wong[5], and Liming Li[6]

[1]Escuela de Ingeniería de Bilbao, Universidad del País Vasco UPV/EHU, Bilbao, Spain, [2]Instituto de Astrofísica de Andalucía, CSIC, Granada, Spain, [3]Department of Physics, Imperial College London, London, UK, [4]NASA Goddard Space Flight Center, Greenbelt, MD, USA, [5]University of California, Berkeley, CA, USA, [6]Department of Physics, University of Houston, Houston, TX, USA

Abstract Jupiter's most intense jet at planetographic latitude 23.7°N experiences vigorous planetary-scale disturbances. The onset consists of the outbreak of 1–3 bright clouds of convective origin developing turbulent plumes. Observed events between 1970 and 2025 shows a cycle of activity with a period in the range of 3.8–5.1 yrs interrupted between 1990 and 2007 by a large period of 17.1 yrs without eruptions. The 2020 and 2025 plumes emerged at the anticyclonic and cyclonic sides of the jet, respectively. They undergo meridional migrations and zonal accelerations during the first 2–3 days of their life, moving toward the jet's peak and exceeded its maximum speed. We propose that interactions between the plume vorticity, the background flow in the jet and planetary vorticity force these meridional motions. A combination of solar radiative forcing of the upper troposphere and convective potential energy build-up at water clouds could generate the cycle.

Plain Language Summary Jupiter's atmosphere periodically undergoes localized eruptions of superstorms due to moist convection in its deep water clouds. They manifest as plumes that trigger a planetary disturbance propagating around the latitude circle from the outbreak position, changing the clouds reflectivity from a zone (high albedo) to a belt aspect (low albedo). Here we study the plumes that take place in the most intense Jovian jet at latitude 23.7°N, examining data from 1970 to 2025. We show that the disturbance occurs quasiperiodically with a period of 4.6 yrs except for a 17.1-year length gap where no plumes were observed (the "plume desert period"). The study of the motion of the plumes of the last two disturbances in 2020 and 2025 shows that they migrated in latitude and accelerated zonally in the first days after their formation, moving toward the peak jet and exceeding its velocity. This study provides key insights into the quasiperiodic and dynamic behavior of Jupiter's most powerful jet, revealing how deep convective processes and jet-plume interactions shape large-scale atmospheric variability. By identifying a quasiperiodic eruption cycle and linking it to both solar forcing and internal energy buildup, the findings offer critical constraints for modeling Jupiter's weather and climate system.

Key Points:

- Jupiter's highest-speed jet at 23.7°N suffers quasiperiodic outbreaks of 1–3 plumes every 4.6 yrs leading to a major disturbance
- The cycle was interrupted by a large period of 17.1 yrs without eruptions when the jet was populated by series of enduring anticyclones
- Plumes form on either north or south of the jet migrating meridionally and accelerating toward the jet peak, exceeding its velocity

Supporting Information:

Supporting Information may be found in the online version of this article.

Correspondence to:

A. Sánchez-Lavega,
agustin.sanchez@ehu.eus

Citation:

Sánchez-Lavega, A., Rojas, J. F., Legarreta, J., Mendi-Martos, A., Hueso, R., Iñurrigarro, P., et al. (2026). The cycles and dynamical properties of convective outbreaks in Jupiter's highest speed jet from a 55-year study. *Geophysical Research Letters*, *53*, e2025GL118481. https://doi.org/10.1029/2025GL118481

Received 29 JUL 2025
Accepted 7 JAN 2026

1. Introduction

Jupiter's North Temperate Belt (NTB) between planetographic latitudes ∼23°N and 31°N contains the highest speed zonal jet in the planet with peak velocities at upper cloud level ∼150–180 ms^{-1} (García-Melendo & Sánchez-Lavega, 2001; Hueso et al., 2017a; Ingersoll et al., 1981; Limaye, 1986; Maxworthy, 1984; Porco et al., 2003; Simon, 1999; Tollefson et al., 2017). From time to time the belt exhibits abrupt changes in its global albedo when transiting from a white zone to a dark belt, through a planetary-scale disturbance initiated by convective plumes (Fletcher, 2017; Pérez-Hoyos et al., 2020; Rogers, 1995; Sánchez-Lavega et al., 2017, 2023; Tollefson et al., 2017; Figures S1–S2 in Supporting Information S1). The phenomenon is known as the NTB Disturbance (NTBD). Albedo changes and dark spot activity in this belt have been documented since 1880 (Peek, 1958; Rogers, 1995). A range of possible periodicities of the NTBD have been reported in the literature, ranging from ∼3.7 to 34.6 yrs, depending on the observation period covered (Fletcher, 2017; Rogers, 1995; Sánchez-Lavega et al., 2008, 2023). However, it was not until 1970 that the first photographic series of a NTB Disturbance (NTBD) involving the presence of a very fast moving bright spot ("a plume") was reported (Reese, 1971). That spot reached the velocity of the peak of the jet as first measured precisely in 1979 by the Voyager 1 and 2. In this paper we present an analysis of all documented cases of plume outbreaks generating an

NTBD, starting with the 1970 case and ending with the last one that occurred in January-February 2025 (a 55-year study), determining their activity cycle. Then we present a detailed analysis of the motions of the plumes of the last two NTBD outbreaks that took place in 2020 and 2025. Finally, we discuss the mechanisms involved in the plume motions and on the cyclic behavior of the disturbance.

2. Data and Methodology

The study of the activity of the NTBD from 1970 to 2016 has been carried out from a reanalysis of the available published data in the visual range (see Table S1 in Supporting Information S1 and references therein). The detailed study of the 2020 and 2025 eruptions is based on images provided by a network of observers around the world, contributing to the repositories of planetary images at ALPO Japan, PVOL (Hueso et al., 2017b), I. Miyazaki's personal archive (see Data Availability) and Hubble Space Telescope (HST) observations (Table S2 in Supporting Information S1). For the NTBD 2020 we have also used images obtained with the PlanetCam camera installed in the 2.2 m telescope at Calar Alto Observatory (Mendikoa et al., 2016). We have used the WinJupos (2024) software to navigate the images and locate the positions of the plumes. Measurements of the photographic records from 1970 to 1990 have position uncertainties in longitude and latitude in the range of ±0.5° to ±1°, (1° in longitude = 1151 km, 1° in latitude = 1125 km) and ±0.5° in ground-based digital images (2007–2025). We analyzed images obtained with the HST in 2019–20 and 2024 (HST, Simon et al., 2015) to obtain the zonal wind profile of the 23.7°N jet using a two-dimensional image correlator (Hueso, 2020; Hueso et al., 2009). Navigation errors in HST images is ±0.1° and in this work we estimate the velocity errors in the range of ±5 ms^{-1}.

3. The NTBD Quasiperiodic Activity From 1970 to 2025

In Figure 1 we show the timeline of the NTBD outbreaks from 1970 to 2025, the number of plumes in each event with their mutual spatial distance, and the time separation between each event (cycle period). In Table S1 in Supporting Information S1 we summarize the main properties of the plume outbreaks and we describe the key characteristics of each event in the following. The first event was a single bright spot photographed on 12 August 1970 and tracked during a month (Reese, 1971). The next outbreak took place in 1975 and involved two plumes, being the first very well documented case of an NTBD thanks to high-resolution photographs (Sánchez-Lavega & Quesada, 1988) and amateur drawings and data (Gómez-Forrellad, 1978; Rogers, 1976, 1990; Figure S3 in Supporting Information S1). The next case occurred in May 1980 following the Voyager 1 and 2 flybys in March and July 1979. It involved two plumes, but the available reports and data are scarce (McKim, 1992; Néel, 1983; Rogers, 1995; Suggs & Beebe, 1980). Next was a missed outbreak that took place during Jupiter's solar conjunction period around 14 January 1985. Photographs before conjunction (up to October 1984) do not show the NTB, but those taken after conjunction (July and August 1985) showed a new and extended, low albedo, reddish NTB (Rogers, 1988; Sánchez-Lavega & Quesada, 1988). An arbitrary outbreak date was assigned to the 1984/85 event due to lack of observations of the exact time of outbreak, as 1985 ± 0.4 with the bounds taken from the period without observations.

The next outbreak was a well studied double plume event in February 1990 (Sánchez-Lavega et al., 1991). Following it, Jupiter images showed no NTBD plume eruption up to 2007. We call this long period of 17.1 yrs without plume outbreaks the "NTBD desert". Between 1994 and 2001, the NTB was a dark belt populated with long-lived anticyclones in the equatorward side of the jet at 23.3°N, close to the jet peak (Figure 1c), moving with an average velocity of 123.9 ms^{-1}, whereas the cyclonic side (poleward) exhibited a complex texture with folded filaments, tilted dark segments and small spots (García-Melendo et al., 2000, 2005; García-Melendo & Sánchez-Lavega, 2001; Simon, 1999). Measurements of the jet profile from 1991 to 2000 based on these HST studies and from Cassini ISS images during its flyby in late 2000 (Porco et al., 2003) showed its peak speed to be low, ∼140 ms^{-1}. In early 2003 the NTB started to fade and the new onset occurred in March 2007 and consisted of two bright plumes that generated a well-studied disturbance that included the first analysis of changes in the shape of the jet profile before and after the outbreak (Barrado-Izagirre et al., 2013; Sánchez-Lavega et al., 2008).

The next eruption took place in April 2012 when Jupiter was approaching solar conjunction. This occurred on 13 May and there are very few, low-quality images capturing just one plume and the early development of the disturbance (Rogers, 2012). The onset of the next disturbance also occurred with Jupiter just 15 days after solar conjunction on 26 September 2016, and was first imaged by the Junocam instrument on the Juno mission in mid-

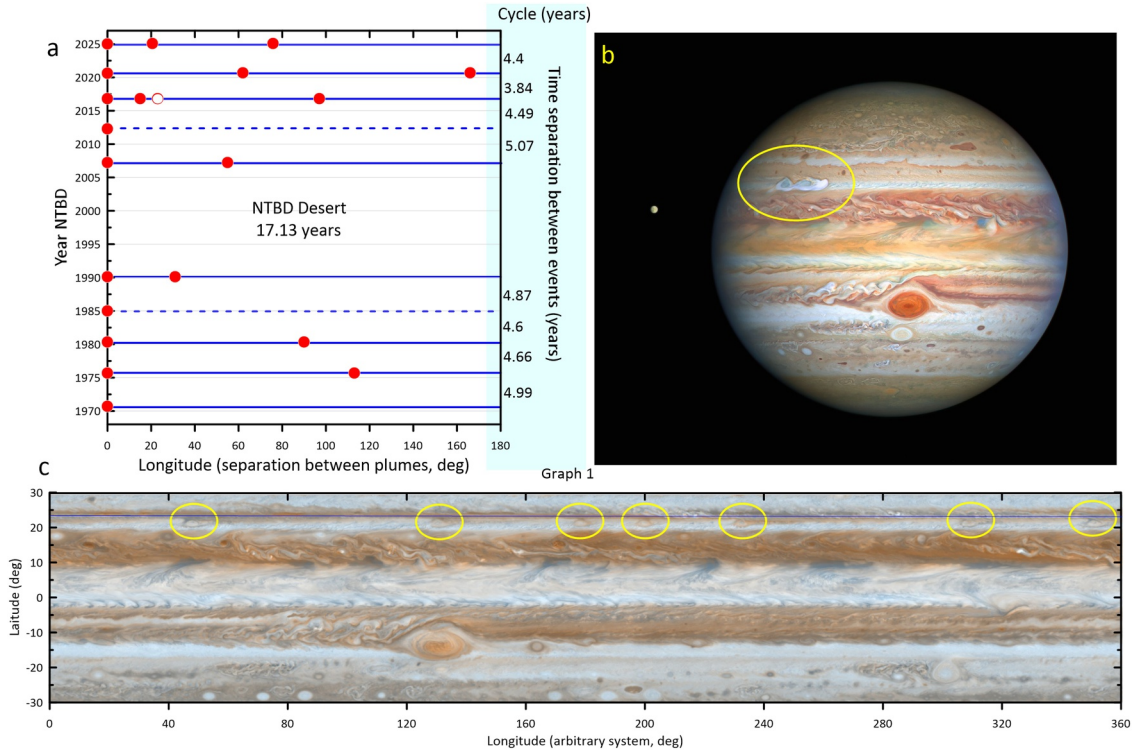

Figure 1. The North Temperate Belt Disturbance (NTBD) plume outbreaks and desert period. (a) The axis show the years (left-y), the periods of the plume cycle (right-y), and longitude separation between plumes for each outbreak (red dots within the blue lines, *x*-axis). Within each outbreak, the longitude separations remained remarkably stable (Figure S3 in Supporting Information S1). The red circle in 2016 indicates the short-lived fourth outbreak that year. The blue dashed lines indicates uncertainty in the date (1985) and uncertainty in the number of plumes (2012). (b) Image of plume P1 and the westward developing wake of the 2020 NTBD (Hubble Space Telescope, 24 August); (c) Cassini ISS map for December 2000 showing the family of anticyclones (yellow circles) during the NTBD desert period and the location of the jet peak (blue horizontal line).

October 2016 (Sánchez-Lavega et al., 2017). The early images showed the presence of four plumes, but one of them seems to have been short-lived as it was quickly destroyed by the zonal disturbance (the wake) generated by the closely located preceding plume. Finally, the next two cases of August-September 2020 and January-February 2025 are studied in detail in next section.

According to Figure 1 and Table S1 in Supporting Information S1, for the 10 outbreaks observed between years 1970 and 2025, excluding the 17.1 year "desert", the NTBD is a quasi-periodic phenomenon with a period range of 3.8–5.1 yrs. We identify two major modes of activity in the NTB and the 23.7°N jet: (a) Cyclic plume outbreaks (typically 1–3 in number) triggering the NTBD showing an average period of 4.6 ± 0.4 yrs; (b) The "NTBD desert" epoch, with no plume outbreaks and with the belt and jet populated with families of oval anticyclones and a variety of cyclonic features (García-Melendo et al., 2000).

4. Plume Dynamics for the NTBD 2020 and 2025

Observations of the plumes at multiple wavelengths from the ultraviolet (0.28–0.38 μm) to the infrared continuum at 1.7 μm show that their brightness is above that of adjacent clouds (Figure S4 in Supporting Information S1). The motions of the plumes from the outbreaks in 2020 and 2025 were very well observed with full temporal coverage of their whole lifetime (Figure 2, Figures S1–S2 in Supporting Information S1). Figures 2a–2d) shows the early aspect of plume P1 in 2020 (we denote the plumes as P1, P2, P3 according to the dates of each outbreak). Plume P1 consisted of two bright spots with a morphology that suggests anticyclonic vorticity (clockwise rotation) (Figure 2d). The aspect of the plumes P1 and P3 in their mature stage is shown in Figures 2e and 2f. The head has a round aspect with a size ∼3,000 km, is covered with patchy clouds and shows a frontal arc-shaped morphology that strongly suggests clockwise rotation.

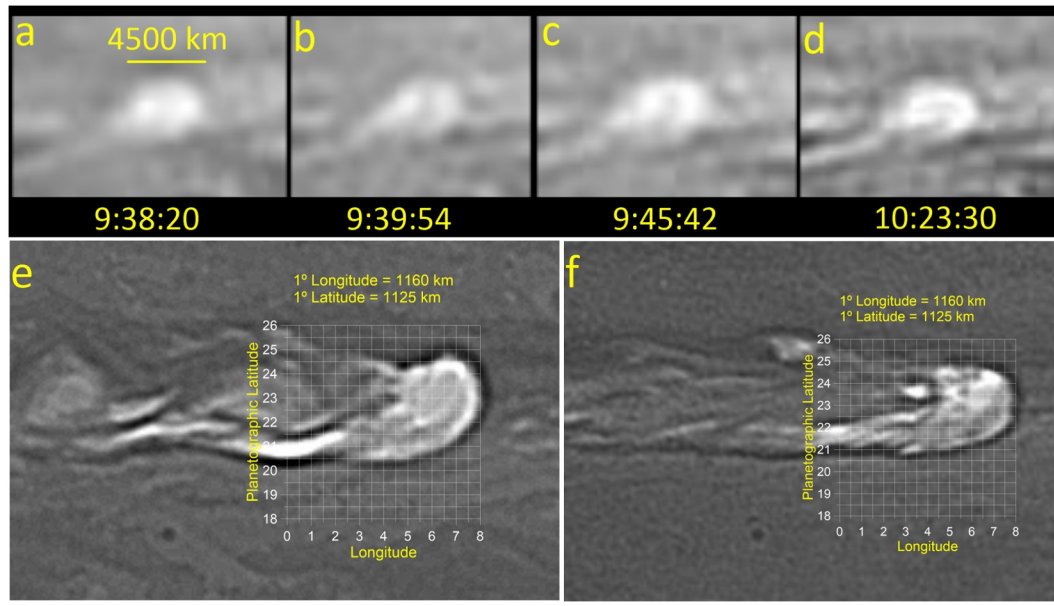

Figure 2. High resolution images of plumes in NTBD2020. The upper file (a–d) shows ground-based images of the very early stage of plume P1 on 19 August. Images by A. Wesley and P. Miles (wavelength ~ 745–950 nm). (e) Plume P1 on 25 August, about 1 week after its outbreak. (f) Plume P3 on 20 September, about 3 weeks after its outbreak. Images (e, f) from Hubble Space Telescope have the brightest parts photometrically saturated (wavelength 889 nm).

The zonal drifts of the 2020 and 2025 plumes relative to System I (rotation period 9 hr 50 min 30 s) is shown in Figure S3 in Supporting Information S1. In Figures 3a–3c and 4a–4c, we show the corresponding zonal velocity for plumes in 2020 and 2025 during their lifetime (Sánchez-Lavega, 2025), using Jupiter's reference rotation System III (rotation period 9 hr 55 min 29.711 s, Archinal et al., 2018). The behavior is the same in all six plumes, regardless of the latitude at which they emerged. Initially, during the first two days, the plumes move with a speed u ~ 130–140 ms^{-1}, accelerating rapidly to a speed u ~ 160–170 ms^{-1} that remained almost constant during their lifetime (~15–60 days). They finally decelerated to speeds u ~ 130–140 ms^{-1} during their demise stage upon interaction with the wake coming from the preceding plume. In the meridional direction all of them initially migrated rapidly in latitude, but the direction depended on the latitude at which the plumes emerged (Figures 3d–3f and 4d–4f). The 2020 plumes outbreak took place between latitudes ~22.4°N and 22.8°N and initially moved in the first days northward (poleward) with a velocity of +1.6 ms^{-1} whereas P2 and P3 showed a steady drift with a velocity +0.4 ms^{-1} during a large part of their lifetime. The 2025 plumes emerged at latitude ~24.4°N migrating during the first 2–3 days southward (equatorward) with speeds of −6.8 ms^{-1}, −7.3 ms^{-1} and −3.7 ms^{-1} (for P1, P2, P3). This meridional migration during the first days of their life coincided in time with their zonal acceleration indicated above.

Figure 5 shows the 23.7°N jet profiles and the plumes locations during both outbreaks (Sánchez-Lavega, 2025). The onset of plumes P1-P2-P3/2020 was south of the jet peak (where the ambient vorticity is anticyclonic), migrating poleward and accelerating eastward simultaneously during the first 1–3 days, i. e. in the direction of the peak of the jet (Figure 5a). Their maximum sustained velocity was u ~ 160–170 ms^{-1}, above that of the jet peak (Figure 5b). Plumes P1-P2-P3/2025 emerged north of the jet peak (where the ambient vorticity is cyclonic), migrating equatorward and accelerating eastward toward the latitude of the peak of the jet (Figure 5c). As in 2020, their maximum sustained velocity was u ~ 160–170 ms^{-1}, above that of the jet peak (Figure 5d). Wind profiles and plume latitudes, albeit less precisely, have been also presented for the 2007 and 2016 cases (Sánchez-Lavega et al., 2008, 2017). In 2007, P1 emerged on the cyclonic side and P2 on the anticyclonic side and both accelerated and migrated toward the jet peak to reach speeds above the jet peak (Sánchez-Lavega et al., 2008). In 2016, the plumes evolved in the anticyclone side and they also reached speeds above the jet peak (Sánchez-Lavega et al., 2017). The conclusion is that plumes migrate meridionally and accelerate zonally during the first days of their lifetime toward the jet peak, independently if they emerged north or south of it, reaching maximum velocities above the jet peak speed and converging on a similar location, just south of the jet stream peak. Figure S7 in

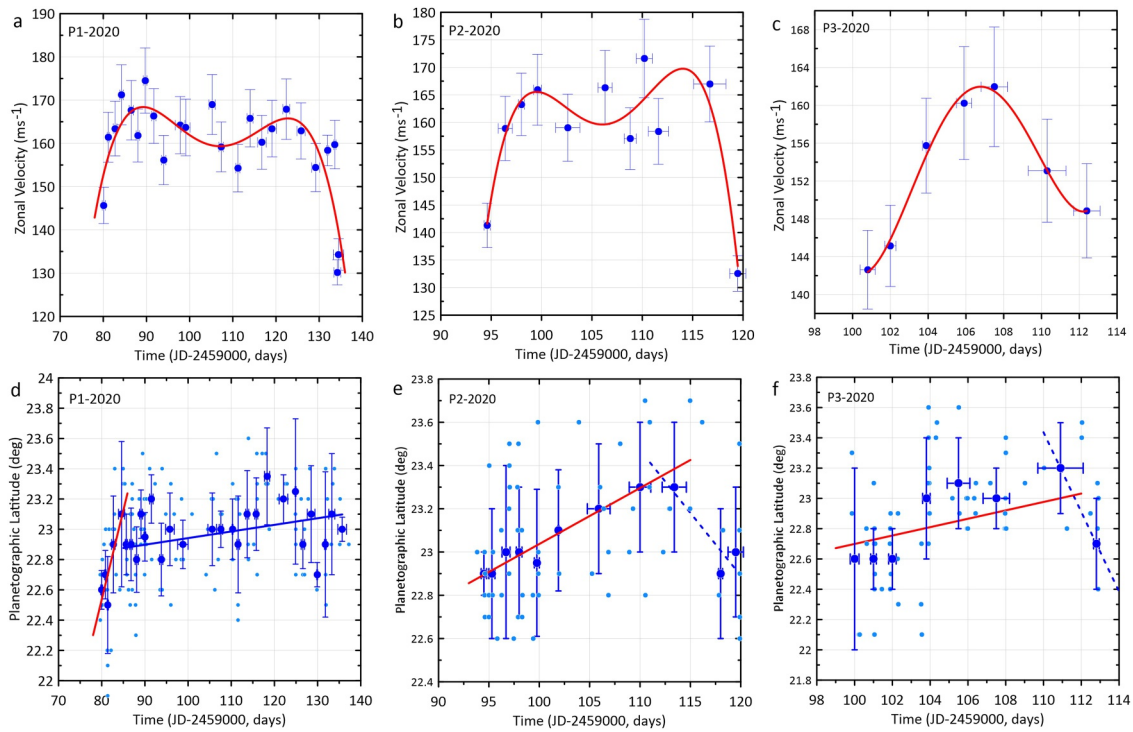

Figure 3. Plume motions (P1, P2, P3) for NTBD2020. (a–c) The zonal velocity for each plume (blue dots) was obtained from the averaged drift rate in blocks of 1–2 days (error bars come from the standard errors of the linear fits to retrieve the velocity). The red curve is a 4-degree polynomial fit to the zonal velocity along the plumes lifetime. (d, e) Latitude migration of the plumes. Individual measurements are shown as small light blue dots. Average latitudes (large blue dots) are calculated in blocks of 1–2 days with the error bars being the standard deviation. The red and blue lines are linear fits for selected periods. For (b, c) the blue dashed line shows a tentative equatorward migration of P2 and P3 during their demise.

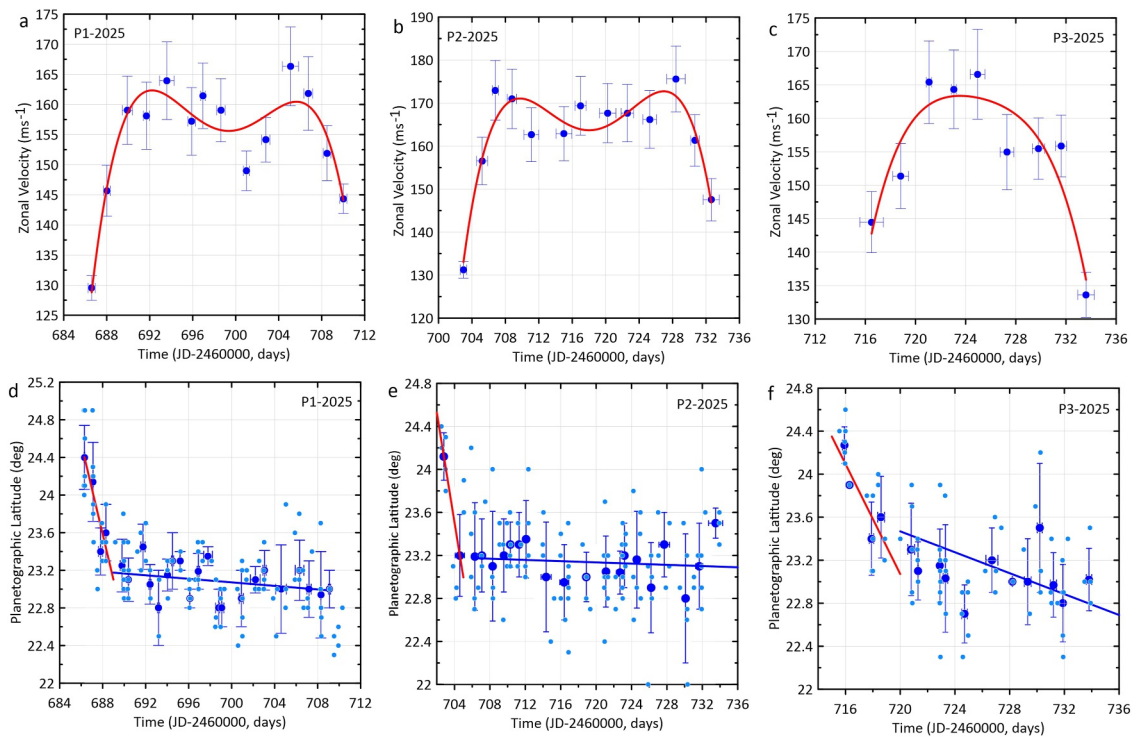

Figure 4. Plumes motions (P1, P2, P3) for NTBD2025. Analysis, color and symbols in this figure are equivalent to those in Figure 3.

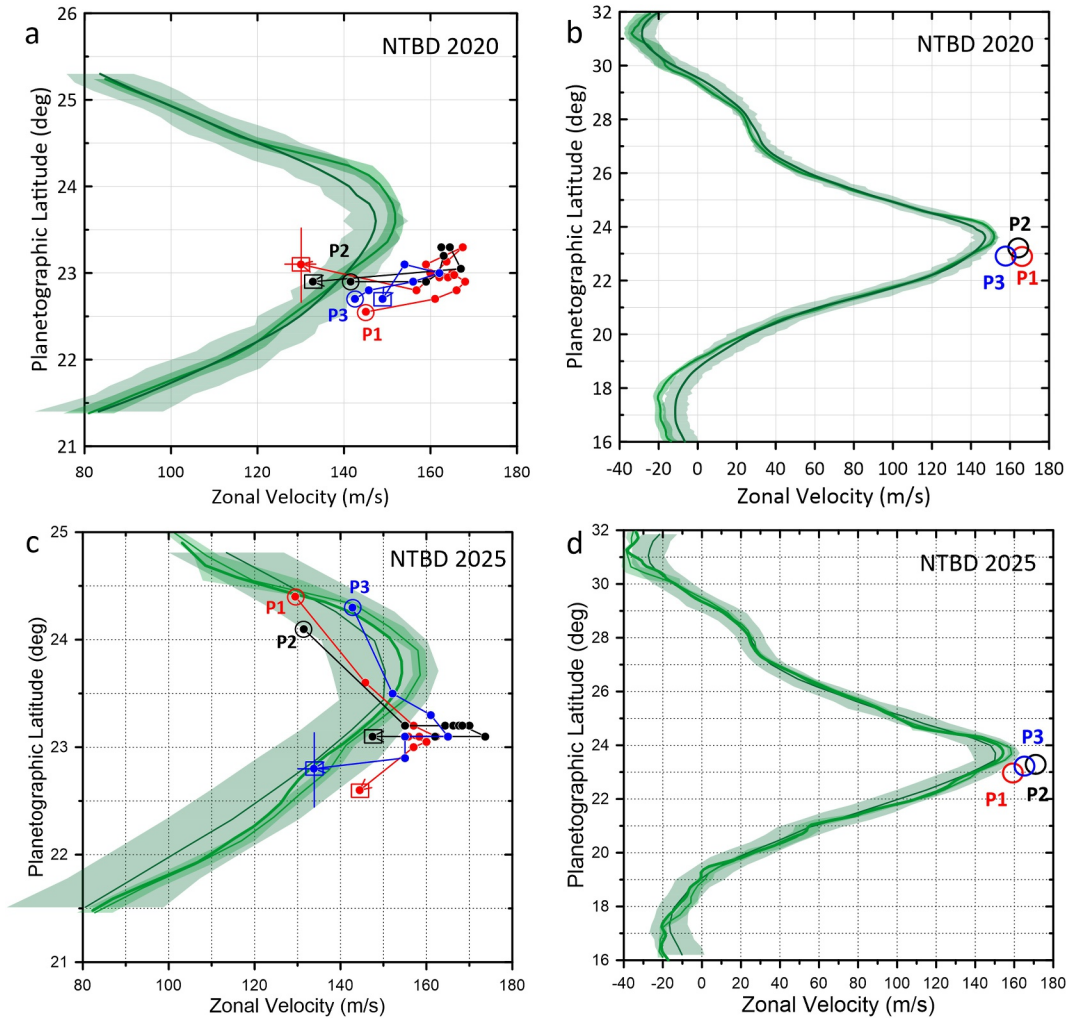

Figure 5. Zonal wind profiles of the North Temperate Belt jet and plumes displacements and location in 2020 (a, b) and in 2025 (c, d), green lines. The shaded areas represents the uncertainty in wind velocity (std from the mean). The jet wind velocity profiles were retrieved from cloud track in Hubble Space Telescope images on 26 June 2019 and 24–25 August 2020 (a, b), and on 19 November 2024 (c, d). The two profiles in panels (a, b) correspond to 2019 and 2020 images, and the three profiles (c, d) for 2024 correspond to images taken with filters centered at wavelengths 467 nm, 631–638 nm, 889 nm. The left panels show an enlargement of the jet peak and the plume motions as indicated by their initial position (dot surrounded by a circle) and final position (dot surrounded by a rectangle) according to the arrow direction. The latitude and wind velocity errors are indicated in one of the dots by the red cross (2020) and blue cross (2025). The right panels show the full jet profiles and plumes location for their maximum sustained velocity (circles). Different colors identify plumes P1, P2 and P3.

Supporting Information S1 shows the plumes motions with velocities relative to background zonal winds and latitude location. They also show an initial acceleration and a final deceleration with a peak speed ~10–30 ms^{-1} above the mean zonal wind.

5. Discussion

As proposed in previous works a plume is assumed to be formed by a system of thermals triggered by water moist convection at a depth ~5 bar (Sánchez-Lavega et al., 2008, 2017). According to the models, the maximum vertical speed of a single updraft of ~100 km in horizontal extent (~4–5 scale heights) is 100–150 ms^{-1}, and develops rapidly in 1–2 hr (Hueso & Sánchez-Lavega, 2001; Hueso et al., , 2002; Sánchez-Lavega et al., 2008). The compact multi-cell plume emerges in the 23.7°N jet that has a half width L_{jet} ~ 6,000 km and a peak velocity u ~ 150 ms^{-1}. This flow is in geostrophic balance according to the Rossby number Ro = u/fL_{jet} ~ 0.18 (Coriolis parameter $f = 2\ \Omega\ \sin\varphi = 1.4 \times 10^{-4}\ s^{-1}$). Since the plume head has a size L_{plume} ~ 3,000 km, a geostrophic

adjustment will occur (Li and Ingersoll, 2015). An estimation of the plume vorticity ζ would be between $f = 1.4 \times 10^{-4}$ s^{-1} and the ambient shear $|\partial u/\partial y| \approx 3 \times 10^{-5} s^{-1}$ (Figures S5a and S6a in Supporting Information S1). The tangential velocity at periphery of each plume is $V_t \sim \zeta\, a/2 \sim 65$ ms^{-1}, where we use a curvature radius a ~ $L_{plume}/2$ and $\varsigma = (f + \partial u/\partial y)/2 \sim 8 \times 10^{-5} s^{-1}$, with sign according to the ambient vorticity. The meridional migration of the plumes could be due to advection of the potential vorticity field (β-$\partial^2 u/\partial y^2$) by the plume circulation (Holland, 1983), neglecting vertical shear. The meridional gradient of the planetary vorticity is $\beta = df/dy = 2\Omega\cos\varphi/R_p = 4.6 \times 10^{-12}$ m^{-1}s^{-1} at 23.7°N but the flow curvature is highly uncertain (Figure S5b, S6b in Supporting Information S1). A crude estimation of the meridional velocity of the plume is $|v| \sim \beta\, a^2 \sim$ 10 ms^{-1} (Holland, 1983) that compares well with the measured values. Plumes emerging in the cyclonic side of the jet move equatorward ($v < 0$), while plumes emerging in the anticyclonic side move poleward ($v > 0$). The initial zonal acceleration (Figures 3,4 and Figure S7 in Supporting Information S1) would be due to the steering component of the motion that drags the plume as it migrates in latitude toward the stronger zonal winds in the jet peak. The steady plume velocity is higher than the measured velocity of the jet peak and this can be explained if the jet has higher speed at deeper atmospheric levels where the plume has its root as previously suggested (Sánchez-Lavega et al., 2008) and from temperature data and thermal wind balance studies (Fletcher et al., 2021). A crude estimate suggests increasing winds at depth with a vertical shear in the range 0.06–0.2 ms^{-1} km^{-1} (Figure S7 in Supporting Information S1). The final plume deceleration is related to its demise (breakdown of the plumes), caused by the interaction with the propagating disturbance from the preceding plume.

Moist convection by latent heat release in hydrogen-helium atmospheres requires special conditions due to the large molecular weight of the condensates (Guillot, 1995; Leconte et al., 2017; Li and Ingersoll, 2015; Li, Ingersoll, Oyafuso, 2018; Li, Jiang et al., 2018; Nakajima et al., 2000; Palotai et al., 2023; Sugiyama et al., 2014). Models of thermals in Jupiter due to water condensation have been show as a viable mechanism to generate the plumes (Aglyamov et al., 2021; Hueso et al., 2002; Hueso & Sánchez-Lavega, 2001). The Convective Available Potential Energy (CAPE) between the level of free convection and the Level of Neutral Buoyancy is given by

$$\mathrm{CAPE} = \int_{z_{LFC}}^{z_{LNB}} g\left(\frac{T' - T}{T}\right) \mathrm{dz} \approx g\left(\frac{\Delta T}{<T>}\right)\Delta z \sim \ 17,800\ \mathrm{Jkg}^{-1},$$

taking ΔT = 2 K for the temperature difference between parcel and environment, $g = 25$ ms^{-2}, and Δz ~ 100 km. An estimation of the time required to store this CAPE in Jupiter's weather layer can be obtained from the thermodynamic conditions and internal heat flux of the planet (C. Li and Ingersoll, 2015)

$$\tau_{\mathrm{thermo}} \approx \frac{C_p\, \Delta P\ \ \Delta T}{F \times g} \sim \ 2.1 \text{ years},$$

for $C_p = 12.36 \times 10^3$ Jkg^{-1} K^{-1}, ΔP = 5 bar (5×10^5 Pa), and internal heat flux $F = 7.485$ Wm^{-2} (Li, Ingersoll, Oyafuso, 2018; Li, Jiang et al., 2018). This period agrees with values estimated by numerical simulations of moist convection for high water abundances of 3–10 times solar (Sugiyama et al., 2014). The radiative time constant in Jupiter's upper troposphere (0.1–1 bar pressure level) is τ_{rad} ~ 4.15 yrs (Conrath et al., 1990). Maximum changes in Jupiter's top of the atmosphere insolation at 24°N are ~ 21% relative to the insolation maximum and occur with a time interval of ~6 yrs (Sánchez-Lavega, 2011; Figure S8 in Supporting Information S1). These time constants are close to the observed period, therefore a combination of radiative heating/cooling of the upper troposphere forced by solar radiation and CAPE build-up at the water cloud level could be involved in the NTBD cycle.

The NTBD is not a global, zonal banded moist convection phenomenon, as is for example, Earth's Intertropical Convergence Zone driven by multiple vigorous cumulus cells (Holton & Hakim, 2013). The outbreak manifests in the form of discrete and latitudinally localized plumes triggered close to the peak of an intense jet. The jet is therefore a key player for the disturbance to develop. The jet must favor a localized concentration of water vapor or modify the thermal structure to overcome critical thresholds to trigger the convective outbreak. Changes in its three-dimensional velocity structure, for example, in its curvature, peak velocity or vertical shear, may favor the triggering of the disturbance. The necessary modeling of the relationship of the jet structure and moist convection (see e. g. Fletcher, 2017; Galperin & Read, 2019; Li et al., 2006; Nakajima et al., 2000; Palotai et al., 2023; Sánchez-Lavega et al., 2017; Sankar & Palotai, 2022; Sankar et al., 2021, 2025; Sugiyama et al., 2014; Young et al., 2019a, 2019b), remains open to future research.

Conflict of Interest

The authors declare no conflicts of interest relevant to this study.

Data Availability Statement

Image measurements were done with the WinJupos (2024) software, which is available at http://jupos.org/gh/download.htm. The PVOL database is accesible at: http://pvol2.ehu.eus/. The ALPO Japan Database is accesible at: https://alpo-j.sakura.ne.jp/indexE.htm. Isao Miyazaki's web page is available at: https://www.ii-okinawa.ne.jp/people/miyazaki/planet/. Hubble Space Telescope images used in this work for the analysis of the 2020 and 2025 events were downloaded from the STScI Mikulski Archive for Space Telescopes Portal at https://mast.stsci.edu/search/ui/#/hst and correspond to HST proposals 15929 and 17294. Data set for Figures 3–5 are published in A. Sánchez-Lavega (2025).

Acknowledgments
This work was supported by Grupos Gobierno Vasco IT1742-22 and by Grant PID2023-149055NB-C31 funded by MICIU/AEI/10.13039/501100011033 and FEDER, UE. P. Iñurrigarro acknowledges support from STFC Grant ST/W001071/1. We are very grateful to the ensemble of amateur observers who submit their observations to databases such as PVOL, ALPO-Japan and the Jupiter section of the British Astronomical Association. A list of contributors is presented in Supporting Information S1.

References

Aglyamov, Y. S., Lunine, J., Becker, H. N., Guillot, T., Gibbard, S. G., Atreya, S., et al. (2021). Lightning generation in moist convective clouds and constraints on the water abundance in Jupiter. *Journal of Geophysical Research: Planets*, *126*(2), e2020JE006504. https://doi.org/10.1029/2020JE006504

Archinal, B. A., Acton, C. H., A'Hearn, M. F., Conrad, A., Consolmagno, G. J., Duxbury, T., et al. (2018). Report of the IAU Working Group on cartographic coordinates and rotational elements: 2015. *Celestial Mechanics and Dynamical Astronomy*, *130*(3), 22. https://doi.org/10.1007/s10569-017-9805-5

Barrado-Izagirre, N., Rojas, J. F., Hueso, R., Sánchez-Lavega, A., Colas, F., Dauvergne, J. L., et al. (2013). Jupiter's zonal winds and their variability studied with small-size telescopes. *Astronomy and Astrophysics*, *554*, A74. https://doi.org/10.1051/0004-6361/201321201

Conrath, B. J., Gierasch, P. J., & Leroy, S. S. (1990). Temperature and circulation in the stratosphere of the outer planets. *Icarus*, *83*(2), 255–281. https://doi.org/10.1016/0019-1035(90)90068-K

Fletcher, L. N. (2017). Cycles of activity in the Jovian atmosphere. *Geophysical Research Letters*, *44*(10), 4725–4729. https://doi.org/10.1002/2017GL073806

Fletcher, L. N., Oyafuso, F. A., Allison, M., Ingersoll, A., Li, L., Kaspi, Y., et al. (2021). Jupiter's temperate belt/zone contrasts revealed at depth by Juno microwave observations. *Journal of Geophysical Research: Planets*, *126*(10), e2021JE006858. https://doi.org/10.1029/2021JE006858

Galperin, B., & Read, P. (2019). *Zonal jets: Phenomenology, genesis, and physics*. Cambridge University Press. https://doi.org/10.1017/9781107358225

García-Melendo, E., & Sánchez-Lavega, A. (2001). A study of the stability of Jovian zonal winds from HST images: 1995 – 2000. *Icarus*, *152*, 316–330. https://doi.org/10.1006/icar.2001.6646

García-Melendo, E., Sánchez-Lavega, A., & Dowling, T. E. (2005). Jupiter's 24°N highest speed jet: Vertical structure deduced from nonlinear simulations of a large amplitude natural disturbance. *Icarus*, *176*, 272–282. https://doi.org/10.1016/j.icarus.2005.02.012

García-Melendo, E., Sánchez-Lavega, A., Gómez, J. M., Lecacheux, J., Colas, F., Miyazaki, I., & Parker, D. C. (2000). Long-lived vortices and profile changes in the 23.7°N high-speed Jovian jet. *Icarus*, *146*, 514–524. https://doi.org/10.1006/icar.2000.6411

Gómez-Forrellad, J. M. (1978). *La Extraordinaria Actividad de la Banda Templada Norte de Júpiter en 1975-76* (Vol. 4). Publicación Monográfica Agrupación Astronómica de Sabadell.

Guillot, T. (1995). Condensation of methane, ammonia, and water and the inhibition of convection in giant planets. *Science*, *269*(5231), 1697–1699. https://doi.org/10.1126/science.7569896

Holland, G. J. (1983). Tropical cyclone motion: Environmental interaction plus a beta effect. *Journal of the Atmospheric Sciences*, *40*(2), 328–342. https://doi.org/10.1175/1520-0469(1983)040<0328:TCMEIP>2.0.CO;2

Holton, J. R., & Hakim, G. J. (2013). *An introduction to dynamical meteorology* (5th ed.). Academic Press – Elsevier. https://doi.org/10.1016/C2009-0-63394-8

Hueso, R. (2020). Particle image correlation velocimetry software PICV3. *Zenodo*. https://doi.org/10.5281/zenodo.4312675

Hueso, R., Juaristi, J., Legarreta, J., Sánchez-Lavega, A., Rojas, J. F., Erard, S., et al. (2017). The planetary virtual observatory and laboratory (PVOL) and its integration into the Virtual European Solar and Planetary Access (VESSPA). *Planetary and Space Science*, *150*, 22–35. https://doi.org/10.1016/j.pss.2017.03.014

Hueso, R., Legarreta, J., García-Melendo, E., Sánchez-Lavega, A., & Pérez-Hoyos, S. (2009). The Jovian anticyclone BA. II. Circulation and interaction with the zonal jets. *Icarus*, *203*(2), 499–515. https://doi.org/10.1016/j.icarus.2009.05.004

Hueso, R., & Sánchez-Lavega, A. (2001). A three-dimensional model of moist convection for the giant planets: The Jupiter case. *Icarus*, *151*(2), 257–274. https://doi.org/10.1006/icar.2000.6606

Hueso, R., Sánchez-Lavega, A., & Guillot, T. (2002). A model for large-scale convective storms in Jupiter. *Journal of Geophysical Research*, *107*(E10), 5-1. https://doi.org/10.1029/2001JE001839

Hueso, R., Sánchez-Lavega, A., Iñurrigarro, P., Rojas, J. F., Pérez-Hoyos, S., Mendikoa, I., et al. (2017). Jupiter cloud morphology and zonal winds from ground-based observations before and during Juno's first perijove. *Geophysical Research Letters*, *44*(10), 4669–4678. https://doi.org/10.1002/2017GL073444

Ingersoll, A., Beebe, R., Mitchell, J., Garneau, G., Yagi, G., & Muller, J. (1981). Interaction of eddies and mean zonal flow on Jupiter as inferred from Voyager-1 and Voyager-2 images. *Journal of Geophysical Research*, *86*(A10), 8733–8743. https://doi.org/10.1029/JA086iA10p08733

Leconte, J., Selsis, F., Hersant, F., & Guillot, T. (2017). Condensation-inhibited convection in hydrogen-rich atmospheres. Stability against double-diffusive processes and thermal profiles for Jupiter, Saturn, Uranus, and Neptune. *Astronomy and Astrophysics*, *598*, A98. https://doi.org/10.1051/0004-6361/201629140

Li, C., & Ingersoll, A. P. (2015). Moist convection in hydrogen atmospheres and the frequency of Saturn's giant storms. *Nature Geoscience*, *8*(5), 398–403. https://doi.org/10.1038/ngeo2405

Li, C., Ingersoll, A. P., & Oyafuso, F. (2018a). Moist adiabats with multiple condensing species: A new theory with application to giant-planet atmospheres. *Journal of the Atmospheric Sciences*, *75*(4), 1063–1072. https://doi.org/10.1175/JAS-D-17-0257.1

Li, L., Ingersoll, A. P., & Huang, X. (2006). Interaction of moist convection with zonal jets on Jupiter and Saturn. *Icarus*, *180*(1), 113–123. https://doi.org/10.1016/j.icarus.2005.08.016

Li, L., Jiang, X., West, R. A., Gierasch, P. J., Pérez-Hoyos, S., Sánchez-Lavega, A., et al. (2018). Less absorbed solar energy and more internal heat for Jupiter. *Nature Communications*, *9*(1), 37009–370018. https://doi.org/10.1038/s41467-018-06107-2

Limaye, S. S. (1986). Jupiter: New estimates of the mean zonal flow at the cloud level. *Icarus*, *65*(2–3), 335–352. https://doi.org/10.1016/0019-1035(86)90142-9

Maxworthy, T. (1984). The dynamics of a high-speed Jovian jet. *Planetary and Space Science*, *32*(8), 1053–1058. https://doi.org/10.1016/0032-0633(84)90062-X

McKim, R. (1992). Jupiter: The apparition of 1979-80. *Memoirs of the British Astronomical Association*, *43*, 39–48.

Mendikoa, I., Sánchez-Lavega, A., Pérez-Hoyos, S., Hueso, R., Rojas, J. F., Aceituno, J., et al. (2016). PlanetCam UPV/EHU: A two channel lucky imaging camera for solar system studies in the spectral range 0.38–1.7 microns. *Publications of the Astronomical Society of the Pacific*, *128*, 035002. https://doi.org/10.1088/1538-3873/128/961/035002

Nakajima, K., Takehiro, S. I., Ishiwatari, M., & Hayashi, Y. Y. (2000). Numerical modeling of Jupiter's moist convection layer. *Geophysical Research Letters*, *27*(19), 3129–3132. https://doi.org/10.1029/2000GL011740

Néel, R. (1983). La Planète Jupiter en 1979-1980. *L'Astronomie*, *97*, 31–45.

Palotai, C., Brueshaber, S., Sankar, R., & Sayanagi, K. (2023). Moist convection in the giant planet atmospheres. *Remote Sensing*, *15*, 219. https://doi.org/10.3390/rs1501021

Peek, B. M. (1958). *The planet Jupiter* (pp. 75–82). Faber & Faber. Chapter 9.

Pérez-Hoyos, S., Sánchez-Lavega, A., Sanz-Requena, J. F., Barrado-Izagirre, N., Carrión-González, O., Anguiano-Arteaga, A., et al. (2020). Color and aerosol changes in Jupiter after a North Temperate Belt Disturbance. *Icarus*, *352*, 114031. https://doi.org/10.1016/j.icarus.2020.114031

Porco, C. C., West, R. A., McEwen, A., Del Genio, A. D., Ingersoll, A. P., Thomas, P., et al. (2003). Cassini imaging of Jupiter's atmosphere, satellites, and rings. *Science*, *299*(5612), 1541–1547. https://doi.org/10.1126/science.1079462

Reese, E. J. (1971). Jupiter: Its red spot and other features in 1969-1970. *Icarus*, *14*(3), 343–354. https://doi.org/10.1016/0019-1035(71)90005-4

Rogers, J. H. (1976). A high-velocity outbreak on the North Temperate Belt. *The Journal of the British Astronomical Association*, *86*, 401–408.

Rogers, J. H. (1988). Jupiter in 1985. *The Journal of the British Astronomical Association*, *98*, 151–164.

Rogers, J. H. (1990). Jupiter, 1973-1977: The pioneer years. *Memoirs of the British Astronomical Association*, *43*, 18–36.

Rogers, J. H. (1995). *The giant planet Jupiter* (pp. 101–110). Cambridge University Press. Chapter 7.

Rogers, J. H. (2012). Major outbreak on NTBs-jet stream. British Astronomical Association Report 2011/12 no. 6. https://alpo-j.sakura.ne.jp/kk12/j120627r.htm

Sánchez-Lavega, A. (2011). *An introduction to planetary atmospheres*. Taylor-Francis, CRC Press.

Sánchez-Lavega, A. (2025). Jupiter NTBD plumes and zonal winds [Dataset]. *Zenodo*. https://doi.org/10.5281/zenodo.18031665

Sánchez-Lavega, A., Irwin, P., & García-Muñoz, A. (2023). Dynamics and clouds in planetary atmospheres from telescopic observations. *Astronomy and Astrophysics Review*, *31*, 5. https://doi.org/10.1007/s00159-023-00150-9

Sánchez-Lavega, A., Miyazaki, I., Parker, D., Laques, P., & Lecacheux, J. (1991). A disturbance in Jupiter's high-speed north temperate jet during 1990. *Icarus*, *94*, 92–97. https://doi.org/10.1016/0019-1035(91)90142-G

Sánchez-Lavega, A., Orton, G. S., Hueso, R., García-Melendo, E., Pérez-Hoyos, S., Simon-Miller, A., et al. (2008). Depth of a strong Jovian jet from a planetary-scale disturbance driven by storms. *Nature*, *451*, 437–440. https://doi.org/10.1038/nature06533

Sánchez-Lavega, A., & Quesada, J. A. (1988). Ground-based imaging of Jovian cloud morphologies and motions: II. The northern hemisphere from 1975 to 1985. *Icarus*, *76*, 533–557. https://doi.org/10.1016/0019-1035(88)90020-6

Sánchez-Lavega, A., Rogers, J. H., Orton, G. S., García-Melendo, E., Legarreta, J., Colas, F., et al. (2017). A planetary-scale disturbance in the most intense Jovian atmospheric jet from JunoCam and ground-based observations. *Geophysical Research Letters*, *44*, 4679–4686. https://doi.org/10.1002/2017GL073421

Sankar, R., Klare, C., & Palotai, C. (2021). The aftermath of convective events near Jupiter's fastest prograde jet: Implications for clouds, dynamics and vertical wind shear. *Icarus*, *368*, 114589. https://doi.org/10.1016/j.icarus.2021.114589

Sankar, R., & Palotai, C. (2022). A new convective parameterization applied to Jupiter: Implications for water abundance near the 24°N region. *Icarus*, *380*, 114973. https://doi.org/10.1016/j.icarus.2022.114973

Sankar, R., Wong, M. H., Palotai, S., & Brueshaber, S. (2025). Wind shear and the role of Eddy vapor transport in driving water convection on Jupiter. *Planetary Science Journal*, *6*(5), 109. https://doi.org/10.3847/PSJ/adcc21

Simon, A. A. (1999). The structure and temporal stability of Jupiter's zonal winds: A Study of the North tropical Region. *Icarus*, *141*(1), 29–39. https://doi.org/10.1006/icar.1999.6163

Simon, A. A., Wong, M. H., & Orton, G. S. (2015). First results from the Hubble OPAL program: Jupiter in 2015. *The Astrophysical Journal Letters*, *812*(1), 55. https://doi.org/10.1088/0004-637X/812/1/55

Suggs, R., & Beebe, R. (1980). A comparison of Recent High-Velocity Jovian Features at 23.5°N Latitude. *Bulletin of the American Astronomical Society*, *5*(8), 685.

Sugiyama, K., Nakajima, K., Odaka, M., Kuramoto, K., & Hayashi, Y. Y. (2014). Numerical simulations of Jupiter's moist convection layer: Structure and dynamics in statistically steady states. *Icarus*, *229*, 71–91. https://doi.org/10.1016/j.icarus.2013.10.016

Tollefson, J., Wong, M. H., de Pater, I., Simon, A. A., Orton, G. S., Rogers, J. H., et al. (2017). Changes in Jupiter's zonal wind profile preceding and during the Juno mission. *Icarus*, *296*, 163–178. https://doi.org/10.1016/j.icarus.2017.06.007

WinJupos. (2024). WinJupos [Software]. Retrieved from https://jupos.org/gh/download.htm

Young, R. M. B., Read, P. L., & Wang, Y. (2019). Simulating Jupiter's weather layer. Part I: Jet spin-up in a dry atmosphere. *Icarus*, *326*, 225–252. https://doi.org/10.1016/j.icarus.2018.12.005

Young, R. M. B., Read, P. L., & Wang, Y. (2019). Simulating Jupiter's weather layer. Part II: Passive ammonia and water cycles. *Icarus*, *326*, 253–268. https://doi.org/10.1016/j.icarus.2018.12.002